MTL TR 88-48

AD

(2)

AD-A205 314

CHEMICAL AND SURFACE CHARACTERIZATION OF TOW MISSILE CASES

SIN-SHONG LIN and WAI K. CHIN
MATERIALS SCIENCE BRANCH

December 1988

US ARMY
LABORATORY COMMAND
MATERIALS TECHNOLOGY LABORATORY

U.S. ARMY MATERIALS TECHNOLOGY LABORATORY
Watertown, Massachusetts 02172-0001

The findings in this report are not to be construed as an official Department of the Army position, unless so designated by other authorized documents.

Mention of any trade names or manufacturers in this report shall not be construed as advertising nor as an official indorsement or approval of such products or companies by the United States Government.

DISPOSITION INSTRUCTIONS

Destroy this report when it is no longer needed.
Do not return it to the originator.

UNCLASSIFIED

SECURITY CLASSIFICATION OF THIS PAGE (When Data Entered)

REPORT DOCUMENTATION PAGE		READ INSTRUCTIONS BEFORE COMPLETING FORM
1. REPORT NUMBER MTL TR 88-48	2. GOVT ACCESSION NO.	3. RECIPIENT'S CATALOG NUMBER
4. TITLE (and Subtitle) CHEMICAL AND SURFACE CHARACTERIZATION OF TOW MISSILE CASES		5. TYPE OF REPORT & PERIOD COVERED Final Report 6. PERFORMING ORG. REPORT NUMBER
7. AUTHOR(s) Sin-Shong Lin and Wai K. Chin		8. CONTRACT OR GRANT NUMBER(s)
9. PERFORMING ORGANIZATION NAME AND ADDRESS U.S. Army Materials Technology Laboratory Watertown, Massachusetts 02172-0001 SLCMT-EMS		10. PROGRAM ELEMENT, PROJECT, TASK AREA & WORK UNIT NUMBERS
11. CONTROLLING OFFICE NAME AND ADDRESS U.S. Army Laboratory Command 2800 Powder Mill Road Adelphi, Maryland 20783-1145		12. REPORT DATE December 1988 13. NUMBER OF PAGES 26
14. MONITORING AGENCY NAME & ADDRESS(if different from Controlling Office)		15. SECURITY CLASS. (of this report) Unclassified 15a. DECLASSIFICATION/DOWNGRADING SCHEDULE

16. DISTRIBUTION STATEMENT (of this Report)

Approved for public release; distribution unlimited.

17. DISTRIBUTION STATEMENT (of the abstract entered in Block 20, if different from Report)

18. SUPPLEMENTARY NOTES

This work was performed under MICOM contract, MTL 7MR00X34N27X46, $14K, covering the period February 4 to April 4, 1987.

19. KEY WORDS (Continue on reverse side if necessary and identify by block number)

Failure analysis, Scanning electron microscopy (SEM),
Surface analysis, Scanning Auger spectroscopy (SAM)
Missile casing, Applied microscopy.

20. ABSTRACT (Continue on reverse side if necessary and identify by block number)

(SEE REVERSE SIDE)

DD FORM 1 JAN 73 1473 EDITION OF 1 NOV 65 IS OBSOLETE

UNCLASSIFIED

Block No. 20

ABSTRACT

Six fragments from TOW missile motor case failures were examined by optical microscopy, scanning electron microscopy, scanning Auger microprobe, and bulk chemical composition analyses. The investigation has identified some positive evidence of corrosion cracking. The inner wall surfaces of the motor casings were corroded and many micro cracks emanating from corrosion pits and oxidized scales were observed. Chlorine was found to be a major element existing in the cracks. Aside from the mechanical strength of the steel, the failure of the motor casings might be attributed to stress corrosion cracking.

INTRODUCTION

The TOW project office (MICOM, Huntsville, AL) requested a representative from the U.S. Army Materials Technology Laboratory (MTL) to join the investigation team on December 16, 1986. The purpose was to investigate the causes of missile case failures by the combined efforts of the U.S. Army Material Command (AMC) laboratories. Mr. C.F. Hickey Jr., from the Materials Producibility Branch (MPB) at MTL, was chosen to be the point of contact (POC) and to coordinate MTL activities with the project office.

The task assigned to MTL included (1) chemical and metallographic analyses of failure pieces from the two sites, and (2) stress corrosion cracking behavior of the C-300 and T-250 unfired missile cases and the C-300, C-250 and T-250 in wrought forms. The contribution of the Materials Science Branch (MSB) is focused on surface and chemical composition analyses of the failure pieces.

Specifically, MSB was assigned to perform:

- Bulk chemical composition analyses of three failure pieces to determine the amounts of titanium, phosphorous, and silicon. In addition, an analysis of hydrogen, oxygen, and nitrogen content was also required.
- Analyses using surface analytical techniques (photo electron spectroscopy, Auger electron spectroscopy, and secondary ion mass spectrometry) to identify all foreign constituents on fracture surfaces, and
- Comparisons of the present results with that of reference materials.

The fragments from the missile cases were made from 18% Ni 300 grade maraging steel[1] (C-300) during the mid and late 1970's. The cases might have been weathered and environmentally corroded in open field for an extended period (1-2 years) before use. Thus, the failure might be related to stress corrosion cracking.

The effort reported here includes the assigned task and the additional studies essential to understand the failure behaviors by available instrumentation in MSB. The work is divided into (1) bulk chemical analyses, (2) optical microscopic (OM) examination of microstructure, (3) scanning electron microscopy (SEM) and energy dispersive X-ray analyses (EDXA) of fracture surfaces, and (4) scanning Auger microprobe (SAM) imaging and Auger electron spectroscopic (AES) identification of elements on fractured surfaces.

EXPERIMENTAL

Six fragments from the failure missile cases were received (through the POC). The pieces were about 2 mm thick and 10 to 20 sq cm, weighing 15 to 30 g, and identified as O-7, O-5, O-13 (Oahu failure); Y-24 and Y-41 (Yakima failure); and B-2 (Blanket test, reference). The sizes and shapes of these pieces are shown in Figure 1.

For analytical purposes, these pieces were cut by a Si C saw blade into several small pieces as shown in Figure 2. The cut pieces are tagged by a letter following their identification. The end cuts which have irregular sizes and large fracture surfaces, are generally reserved for uses in OM, SEM, and SAM surface studies, and the large cuts are used for quantitative chemical composition analyses. For the latter analyses, the pieces are further chipped and ground by the MTL machine shop. The distribution of the cut specimens for analyses is tabulated in Table 1.

Table 1. DISTRIBUTIONS OF SAMPLES FOR ANALYSES

Bulk Chemical Composition	Microstructure by OM	Fracture Surface by OM, SEM & SAM
B-2a	B-2c	B-2e
Y-41d	Y-41b, 41f	Y-41a
Y-24b	Y-24d, 24e	Y-24e
O-13c	O-13b	O-13e
O-7c	O-7b	O-7e
O-5d	O-5c	O-5a

1. DECKER, B.F., EASH, J.T., and GOLDMAN, A.J. *18% Nickel Maraging Steel.* ASM Transaction Quarterly, v. 55, 1962, p. 58.

Quantitative chemical composition analysis was carried out by the inductively-coupled argon plasma (ICAP) atomic emission spectrometer made by Jarrell Ash Co., Model 955. For microstructure analyses, the cross sections of the specimens were examined after grinding and fine polishing. The metallographic photos of the surface treated with a mild etching solution ($CuCl_2$-HNO_3-HCl) were taken under polarized light. The fracture surfaces are analyzed by OM at a low magnification, followed by SEM, AMR model 900 F4, and SAM, PHI model 548.

RESULTS

Quantitative Chemical Composition Analysis

The elemental compositions of the maraging steels were quantitatively determined by ICAP, oxygen and nitrogen by the LECO inert gas fusion apparatus, and carbon and sulfur by the LECO combustion method. The calibration was made against NBS 1156 steel. As shown in Table 2, minor variations of chemical compositions are observed, but no high abnormality is found.

Table 2. CHEMICAL COMPOSITION OF FAILURE PIECES

	Composition (weight %)														
Sample	Ni	Co	Mo	Ti	Cr	Mn	Si	Al	Cu	P	B	C	S	N	O
														(- ppm -)	
NBS-1156	19	7.3	3.1	0.21	0.20	0.21	0.18	0.05	0.02	0.011	0.003	0.023	0.012		
#B-2	18.2	8.7	4.8	0.86	0.04	0.20	0.12	0.08	0.09	0.008	0.004	0.039	0.001	4	25
#Y-41	19	9.3	4.9	0.83	0.01	0.22	0.09	0.08	0.04	0.011	0.003	0.044	0.002	2	26
#Y-24	18.9	9.2	4.9	0.85	0.01	0.22	0.09	0.08	0.02	0.011	0.003	0.016	0.002	2	36
#O-13	18.6	9.5	4.9	0.83	0.005	0.22	0.10	0.08	0.02	0.011	0.003	0.013	0.001	4	67
#O-7	18.5	9.1	4.9	0.82	0.005	0.21	0.07	0.08	0.03	0.011	0.003	0.013	0.001	<1	27
#O-5	18.1	9.0	4.8	0.80	0.005	0.20	0.11	0.08	0.03	0.008	0.003	0.015	0.001	4	85
Range	17-19	7-8.5	4.6-5.1	0.3-0.5	-	0.1*	0.1*	0.1†	-	0.01*	0.003†	0.003*	0.01*	-	-

*: Maximum
†: Added

OM Cross-section Analyses

The polished cross sections of the six samples were examined by OM at 500X. This investigation was focused on two areas: the evidence of crack formation and the microstructure of the steels. Specifically, the emphasis was directed to locating the origin, initiation and growth of microcracks from corrosion pits or crevices on the inner surfaces. Therefore, the cross-section cuts were made across corroded regions on the inner wall. However, not every cross section revealed the existence of corrosion cracks.

As shown in Figure 3, a few cracks are positively identified in the specimens from the two sources. In both instances, the microcracks are found to emanate from pits or crevices situated on the inner cylindrical wall. In general, these observed cracks extend approximately 20 micron depth from the surface, and have zigzag passages presumably through grain boundaries of the steel structure. The widths of the cracks are less than a few tenths of a micron. No fissure or crack is observed from the smooth inner surfaces. Evidently, the formation of these cracks is corrosion related.

The polished cross sections were examined under a polarized light after etching as shown in Figure 4. The grains on the order of 10 μm are elongated and oriented along the direction of swaging and rolling. The textures of #O and #Y samples are very similar, but those of #B samples are slightly different. The #B reference sample is found to consist of slightly larger grains. Some strips of darker regions are observed, which might come from staining and discoloration from the etching solution.

OM Analyses of Fracture Surfaces

The five samples obtained from the two failures showed considerable visible corrosion on the inner surfaces, but none was observed on the outer surfaces. As shown in Figure 5, the extent of inner surface pitting and oxide scale formation from Oahu and Yakima failures were different. The topology of the first source was dominated by a large amount of pitting, and the second one by an extensive scale formation. The density of pitting and the dimension of oxide scales

varied widely for each specimen (presumably depending on locations). The reference specimen #B-2a showed no detectable scale and pitting.

The OM photos (Figure 6) show unique characteristics of the fracture surfaces. Most of the surfaces are brown rusty patches with some spotty gray lusters. Three specimens from Oahu show different failure behaviors. The fractures of specimens #O-5a and #O-13e mainly resulted from a catastrophic burst with many cracks and seams running across the thickness. The apparent differences are observed only in the extent of rust formation in these two fractured surfaces. The surface of #O-5a has more oxidized scales and that of #O-13e has many localized rusty pits. In addition to the rust formation, the surface of #O-7e has many strain failure cracks running parallel to the wall.

The two fracture surfaces of the Yakima specimens, #Y-24 and #Y-41, are very similar. The cracks on the surfaces are not as visible as compared to those of the Oahu samples. The surfaces are less rugged, and rust is more localized and situated near the inner wall.

The reference specimen #B-2 has an interesting surface morphology. The fracture topology, in addition to numerous cracks, is found to contain many inclusions, precipitates or particles (appeared as black) protruding from the fracture surface. These features are later identified as foreign contaminants by SEM, SAM, and EDXA.

Fracture Surface Analyses by SEM and EDXA

The fracture surfaces of six samples were examined by SEM followed by EDXA for composition analysis. Much contamination, oxide layers, precipitates, and aerosol particles were observed on the surfaces, and some of their chemical constituents were identified. The chemical constituents of these fracture surfaces obtained from EDXA analyses are tabulated in Table 3. The sampling locations in the first column are shown on the SEM images of the respective specimens, (Figures 7-12). The surface morphologies differ slightly from piece-to-piece and the brief descriptions are given below:

#O-5a: The surface of this sample has been weathered and oxidized to a considerable extent. In the SEM photos (Figure 7), a protruded crack surface is shown. This cracked surface is highly oxidized and appears as brown coloration (from OM color photo, Figure 6) in contrast to bright metallic luster. Many small aggregations shown on the SEM photo are oxidation products. Subsequent EDXA analyses of the four spots reveal that there are high concentrations of K, Na, and Cl near the surfaces adjacent to the inner wall (#3, #2, and #1), especially at the edge of the boulder (spot #1, EDXA spectrum is shown). In contrast to the flat smooth portion of the fracture surface (#4) where no salt element is detected, these spots contain excessive amounts of Cl.

#O-7e: The surface is found to have several strain fracture cracks running parallel to the cross section. The surface appearance is rusty brown with numerous fractures and cracked lines and edges. Some portions are rugged and others smooth, as shown in Figure 8. Composition analyses were made on four locations as indicated in the figure. The elemental constituents of these spots are very similar except for varying small concentrations of K and Cl.

#O-13e: This unique fracture surface (Figure 9) consists of many spots appearing as dark circular areas in the SEM photos (brown/black spots in OM photos, Figure 6). Presumably, these spots are preferentially oxidized portions of steel components. EDXA analyses indicate that they are mainly composed of maraging steel components with varying amounts of minor elements Al, Cr, and Ca. No Cl is detected.

#Y-24e: The fracture area as shown in Figure 10 is oxidized to many localized brown patches throughout the surface. The EDXA analyses of the extruded crack ridge surface near the inner wall (#1 through #3), reveal that only #1 spot contains a small concentration of Cl. No Cl is detected on the adjacent two spots (#2 and #3). The enlarged area at the center (#4) shows that the surface is highly oxidized. The chemical compositions of all spots from EDXA are similar to the maraging steel except for relative abundances.

#Y-41a: The surface morphology (Figure 11) of this specimen is very similar to that of #Y-24e. The spot (#1) on the cracked surface near the inner wall shows the presence of Si, K, Cl, and Al in addition to the elemental steel constituents, but the adjacent spots (#2 and #3) show only the components of the maraging steel. The occurrences and distribution of these exotic elements suggest they are derived from contamination.

#B-2e: This surface is distinctly different from the two failure samples. Numerous small particles (about 20 μm or less) were found to fuse and to embed on the fractured surface (Figure 12). The particle with round corners and edges (#4) is found to contain large amounts of Cu and Pb, while those with sharp edges (#3) have high contents of Al and Mo as compared to the metal compositions of the maraging steel (#1 and #5). EDXA spectra of spots #3 and #4 are shown in the figure. No Cl is found throughout the surface.

Table 3. CHEMICAL CONSTITUENTS OF FRACTURE SURFACES BY EDXA

Sample/Locations		Elements Detected by EDXA											
		Na	Al	Si	Mo	Cl	K	Ti	Fe	Co	Ni	Cu	Pb
#O-5a	#1	243	333	613	412	2201	2833	†	654	*	*	†	†
	#2	†	1203	1974	970	931	1076		11419		1792		
	#3		396	480	2877	1298	1228	740	3971		1436		
	#4			301	894			309	18919		2439		
O-7e	#1					†	744	†	5509		420		
	#2				856	†	†	248	11162		1968		
	#3					237	227		5760		1138		
	#4							†	6653		625		
#O-13e	#1		92	†	†	†	†		2456		302		
	#2		181	†	334	†	†	†	5592		941		
	#3							†	3167		355		
	#4		273		313			†	5174		1982		
	#5		321		553			†	6705		1094		
#Y-24e	#1				443	174	†	†	2261		161		
	#2				247			†	4223		714		
	#3							†	4371		726		
#Y-41a	#1		340	801	808	179	278	294	3626		343		
	#2		360						6572		1034		
	#3				623				9657		1505		
#B-2e	#1				516			†	7194		1559		
	#3			1018	521			†	1822		240		
	#4			191				†	483		*	972	2321
	#5			179	712			†	5961		913	†	†

* Presented but not recorded due to overlapping signals.
† Not observed or present in minute amounts.
Numbers are counts/min, and for relative comparison only, not in an absolute scale.
Locations/# spot are shown in SEM of Figures 7 through 12.

Fracture Surface Imaging by SAM

The samples as-received were heavily contaminated and oxidized, therefore, true nature of the fracture surfaces was hard to determine. In the SAM imaging, the major constituents of the steel such as Fe, Ni, and Co as well as other exotic elements were recorded. Since the study is focused on the confirmation of corroding chemicals such as Na, Cl, and S and their spatial distributions, only those elemental images relevant to the two discussions are presented below:

#O-5a: In addition to the elemental constituents of maraging steel, a few foreign elements are observed on the fracture surfaces. They are Cl, O, and N. Oxygen is a component of oxidized metal layers and nitrogen probably derived from propellant remains on the surface. The distribution of Cl is rather unique. As shown in Figure 13, the high concentrations are observed near rims and edges of the cracked surface adjacent to the inner wall, and the two pits situated on the inner wall. No Cl is observed away from the inner wall. The presence of Cl is also confirmed by AES spot analysis. The element is one of the chemicals known to cause stress corrosion cracking.[2]

#O-7e: The SAM imaging is obtained on the region containing a strain crack. As expected, the surface is highly oxidized and contaminated. Several concentrated Cl sites are observed as illustrated in Figure 14. The SAM imaging and analyses also revealed a widespread concentration of K. These K and Cl sites are widely scattered and they could only be derived from the surface contamination by the missile propellant. Two AES spectra illustrate the magnitude of Cl on two different locations.

2. SYRETT, B.C. *Stress Corrosion Cracking in 18% Ni (250) Maraging Steel.* Corrosion, NACE, v. 27, 1971, p. 216.

#O-13e: Only one Cl concentrated site is detected on the SAM imaging. This location is at the half wall thickness and is not near the inner cylindrical wall of the casing as shown in Figure 15. This Cl origin is not clear, but it could come from propellant contamination.

#Y-24e: This sample obtained from Yakima failure exhibits several Cl concentrations on the fracture surface. Most of the Cl is aggregated near the inner wall as shown in Figure 16. The AES spectra clearly confirm the presence of Cl.

#Y-41a: No Cl is observed in the imaging area of this sample. The fracture surface (Figure 17) is mostly oxidized and contaminated with nitrogen/NO containing hydrocarbons. A large Ca signal is observed in one of AES spectra (not shown) obtained from this area.

#B-2a: This reference (blanket test) sample shows no Cl element on the fracture surfaces. Instead, many exotic elements such as Cu, Sn, S, Si, and Al are observed. Al and Si are present in excess of the steel components and Cu and Sn are found to scatter widely. Those metals are probably derived from aerosol particles during explosion. Sulfur always coexists with oxygen and is probably presented as sulfate or sulfite. Only Cu elemental distribution is shown in Figure 18 together with three AES spectra containing those foreign metals.

DISCUSSION

Quantitative Chemical Composition Analysis

The composition of the reported maraging steel containing 18% Ni are tabulated in Table 4 for comparison with the present quantitative chemical composition analyses (Table 2). The four important constituents, Ni, Co, Mo, and Ti, are within the acceptable composition ranges of 18% Ni maraging steel. The nitrogen and oxygen contents are so minute that some of them are probably derived from surface residues and contamination. The carbon concentration is higher than the maximum limit but is not far away from the NBS sample. The amount of titanium is slightly higher but it has no substantial detrimental effect on the strength of the steel. Judging from the small amounts of C and N, the thermal embrittlement[3] caused by Ti (C,N) precipitates in austenite grain boundaries is minimal. Thus, the mechanical properties of these three failure specimens are believed to be very similar.

Table 4. MAJOR METAL CONSTITUENTS OF MARAGING STEEL (Ref. 1)

Alloy	Composition (wt%) Ni	Co	Mo	Ti	Yield Strength (ksi)
18Ni 250	18	8	5	0.4	250
18Ni 200	18	8	3	0.2	200
18Ni 300	18	9	5	0.7	300

OM Cross Section Analyses

Two significant observations are made from the present OM cross-sectional analyses: (1) the presence of microcracks emanating from corroded spots on the inner wall, and (2) the grain morphologies of the maraging steels. Attempts also have been made to identify differences among the microstructures of the steels derived from three sources.

For stress corrosion cracking, the crack initiation is usually derived from the environmentally corroded surfaces. Therefore, special attention was placed on identifying surface fissures and cracks from the cross-sectional microphotographs. In order for a crack to be detected, the cross-sectional cut must be made across the crack initiation areas. In Figure 3, some surface intrusions of corroded areas from the inner wall were observed, but only a few definite patterns of microcracks or fissures emanating from corroded surfaces were detected. These microcracks penetrated to a depth of 30 μm below the surface. The significance of this finding implied that there might be many larger corrosion

3. KALSH, D., and RACK, H.J. *Thermal Embrittlement of 18 Ni (350) Maraging Steel.* Metallurgical Transactions, v. 2, 1971, p. 2662.

cracks extending to a few hundreds of microns depth below the surface. The existence of the microcracks clearly demonstrates that stress corrosion cracking is possible.

In Figure 4, the etched surfaces are shown. All grains were found to align and elongate presumably on the direction of rolling and swaging. The grain structures of the three sources are not very much different. Thus, the compositions and the heat treatments of these steels are believed to be fairly similar.

OM Fracture Surface Analyses

As shown in Figure 6, the cracked surfaces are heavily corroded with air/moisture and the surface compositions might have been altered. The investigation is further complicated by these environmental factors, as well as contamination during handling. Moreover, information derived is fragmentary due to the few pieces available for analysis.

The fracture mechanism of a thin cylindrical wall proceeds through the fissures or microcracks (or artificial flaws) initiated from the inner surface. The crack growth would occur initially in the thickness direction and when it had penetrated the wall, it would grow lengthwise. In the piece O-7e, several strain cracks situated at a half wall thickness were observed. This observation suggests that the catastrophic fracture might occur under predominantly the plane strain condition. During the crack growth, shear lips were formed. The propagation of shear lips creates internal cracks. Eventually the fully developed fracture occurred by shear. Some portions of received samples are remnants of shear pieces with only a half wall thickness.

The corrosion cracks derived from surface pits and crevices are hard to identify on the present fracture surfaces. These cracks are formed along grain boundaries and are indistinguishable from the cracks derived from the catastrophic (fast) intergranular fracture. Only the detailed examination of surface morphology could be used to distinguish the difference. Since the fracture surfaces are already oxidized and contaminated, the separation of these two cracks is almost impossible. The confirmation of foreign corrosive elements existing on the fracture surfaces is the only method of confirmation (see EDXA and SAM analyses).

Fracture Surface Analyses by SEM and EDXA

The morphological features as determined by SEM and the chemical composition analyses carried out by EDXA has revealed a significant phenomenon concerning fracture behavior of two failure samples. The morphological features observed by SEM are mostly oxidized laminated layers with appearances of hydrogen/water intrusions. Under a high magnification, some layers are loose scales with interconnecting pores and voids (Figures 10(c) and 11(b)). The chemical composition analyses of microdomains by EDXA indicated the presence of many foreign chemical elements.

The foreign elements observed from three sources are significantly different: the failure pieces of Oahu and Yakima contained K, Si, S, and Cl while the reference piece contained Sn, Pb, Si, and Cu, in addition to O and N. The most important corroding element, Cl, was localized and presented in the failure pieces, but it was not detected in the reference sample. The Cl contamination was mainly distributed near the inner cylindrical wall and on some fracture surfaces presumably formed from corrosion cracks along grain boundaries. Sulfur was found to be present in a minute quantity. Since a large amount of oxygen is always associated with sulfur, S probably exists as a highly oxidized state of sulfate or sulfite.

The exotic elements Cu, Pb, Sn, and excessive amounts of Al and Si detected on the #B fracture surfaces are presumably derived from debris during the catastrophic failure. From SEM image analysis, those elements are surface contaminants and are probably derived from impacts during explosion. Potassium that is frequently observed, could be either an artifact of SEM analysis or derived from the missile propellant.

Fracture Surface Imaging by SAM

From the imaging and composition analyses[4] by SAM, the fracture surfaces of the two failure samples, Oahu and Yakima, revealed the presence of a corroding agent Cl on the surface. In three specimens from Oahu and one from Yakima, Cl is present on the fracture surfaces. The majority of Cl is found to distribute near the inner wall, and is

4. LIN, S.S. *Chemical Constituents of Eroded Gun Surfaces.* Application of Surface Science, v. 21, 1985, p. 112.

concentrated on the rims and the edges of the cracked surfaces. In some cases, a small amount of S is also detected. Sulfur could exist as sulfate ($SO_4^=$) possibly coming from acid rain. The presence of Cl in the cracked surface strongly suggested that microcracks are formed by Cl and, to a lesser extent, by $SO_4^=$. Potassium which is probably precipitated from the missile propellant, is occasionally observed but does not coexist with Cl.

In contrast, no Cl is detected in the reference sample, #B-2a. But many foreign elements like Cu, Sn, and large amounts of Al and Si oxides, are observed in the surface. They probably come from debris after explosion and are not from chemicals originally presented in the steel.

Some of the chlorine could be derived from the oxidizing component of the propellant $KClO_4$. The Cl precipitation might have occurred after the catastrophic failure. If this was the case, then the SAM Cl image should have a wide distribution similar to K or any component of the propellant. The fact that Cl is more concentrated on the fracture surface near the edges of the inner wall implied that these Cl were present before the failure.

CONCLUSIONS

The failure of the cylindrical missile casing could be attributed to one of two causes: (1) the specified mechanical strength of the maraging steel used in the fabrication of the motor cases, and (2) the existence of corrosion cracks induced by environmental factors under a high stress.

The 18% Ni 300 grade maraging steel used in the casing should produce a yield strength of 300 ksi. The annealing temperatures as well as the processing parameters of the steel would influence the extent of thermal embrittlement caused by excessive precipitates Ti(C,N) on austenite grain boundaries. The present OM microstructure analyses at a low magnification could not determine the extent of the precipitation, and there was no observable difference or a large abnormality among three grain structures. Moreover, the bulk chemical composition analyses also indicated that there is no significant composition difference between the failure samples and the composition of the maraging steel (Tables 2 and 4). The thermal embrittlement fracture might be another cause of the failure, however this is very unlikely from the present composition analysis.

The failure might be derived from stress corrosion cracking.[2,5] The stress corrosion cracking must be initiated from surface fissures, microcracks or processing flaws which could be catastrophically fractured under high stress. The surface fissures or environmentally induced cracking is dependent on such parameters as pH, NaCl concentration, corrosion potential, temperature, and time duration. The formation of surface fissures is initiated either from anodic path dissolution or hydrogen embrittlement, and the cracks are usually grown along austenite grain boundaries until a catastrophic fracture.

The present investigation has found some evidence of stress corrosion cracking: the presence of corroded pits, crevices, and scales on the inner wall surface, the existence of microcracks propagating along grain boundaries and emanating from the surface pits, and the positive identification of the corroding elements Cl and S ($SO_4^=$) on the fracture surfaces. The depth penetrations of the observed microcracks were in the range of 20 microns. However, there might be larger and longer cracks extending one tenth of the wall thickness which were not detected. This stress corrosion cracking would be initiated from the surface by moisture and acid in humid atmospheres. However, the catastrophic fracture would not occur if the strength of the maraging steel exceeded the specification of 300 ksi and the corrosion cracks were insignificant. In some fragments, the strain fracture pattern formed by shear lips during explosion was observed.

The corrosion pits on the inner wall observed by OM might be formed during storage and shipping after the missile failure. This possibility exists since the fracture surfaces had been heavily oxidized and contaminated. If this was the case, then the fracture surface should have exhibited a similar extent of pittings (or a greater extent due to the freshly exposed metal surface) as that of the inner wall surface. However, the pitting was not detected. Moreover, the distribution of Cl on the fracture surface from SAM data suggested that the pit formation after the failure is an unlikely event. The artificial flaws from improper processing might be presented and might not be detected. This could be an unexpected cause of the failure.

5. PARKINS, R.N., and HANEY, E.G. *Stress Corrosion Cracking of 18 Pct Ni Maraging Steel in Acidified Sodium Chloride Solution.* Transactions of the American Institution of Metallurgical Engineers, v. 242, 1968, p. 1943.

This report described only the results from the chemical (bulk and surface) compositions and the metallographic investigations in which corrosion cracks were identified. The final conclusion should depend on the mechanical strength testing.

ACKNOWLEDGMENT

The technical assistance of R. Jurta, J. Donnelly, and G. Meyers for the OM and SEM works are highly appreciated.
preciated.

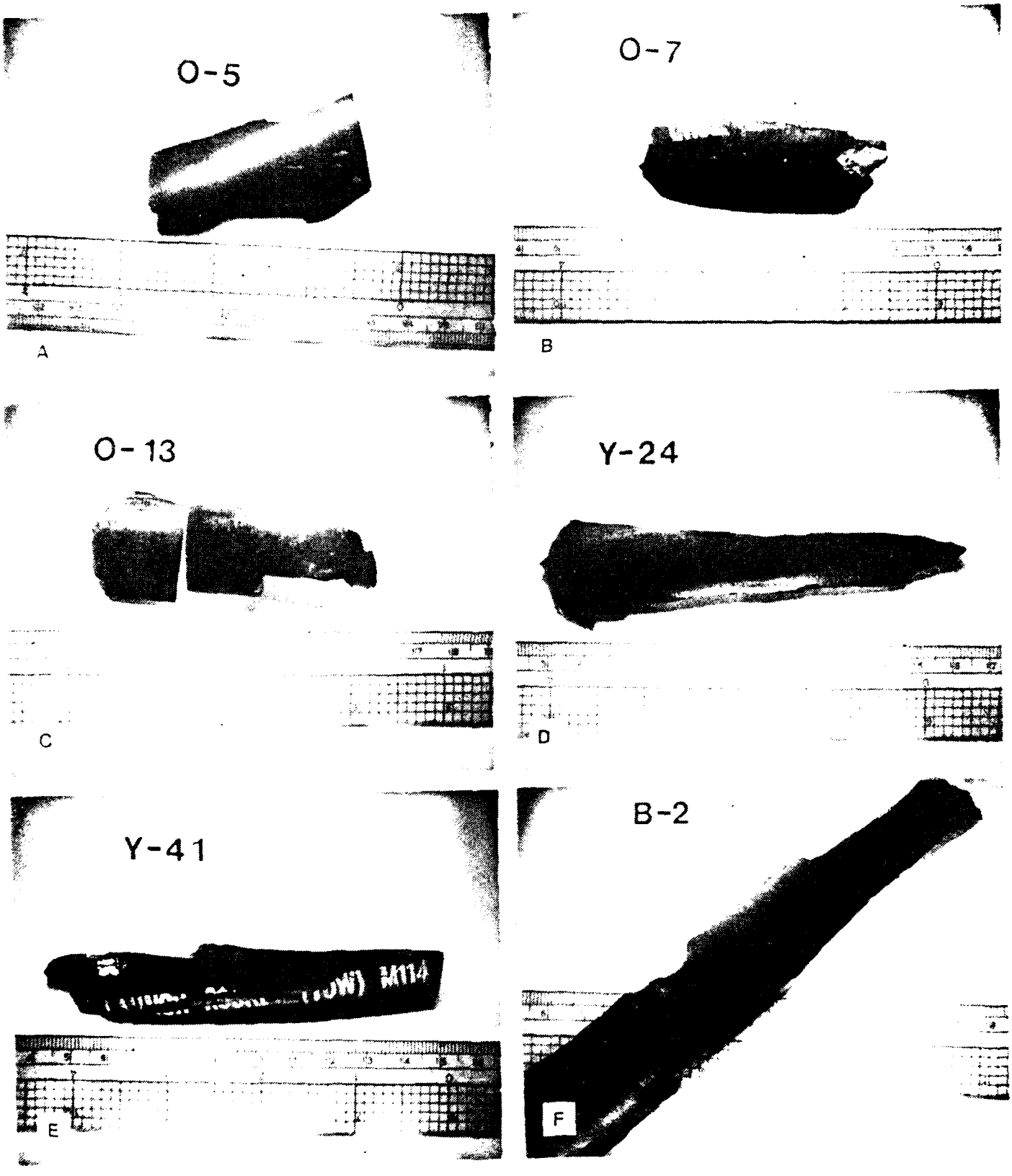

Figure 1. Fracture pieces from missile case failure. Six samples were received from three sources. Oahu, Yakima and Blanket test (reference). (a) #O-5 (b) #O-7 (c) #O-13 (d) #Y-24 (e) #Y-41

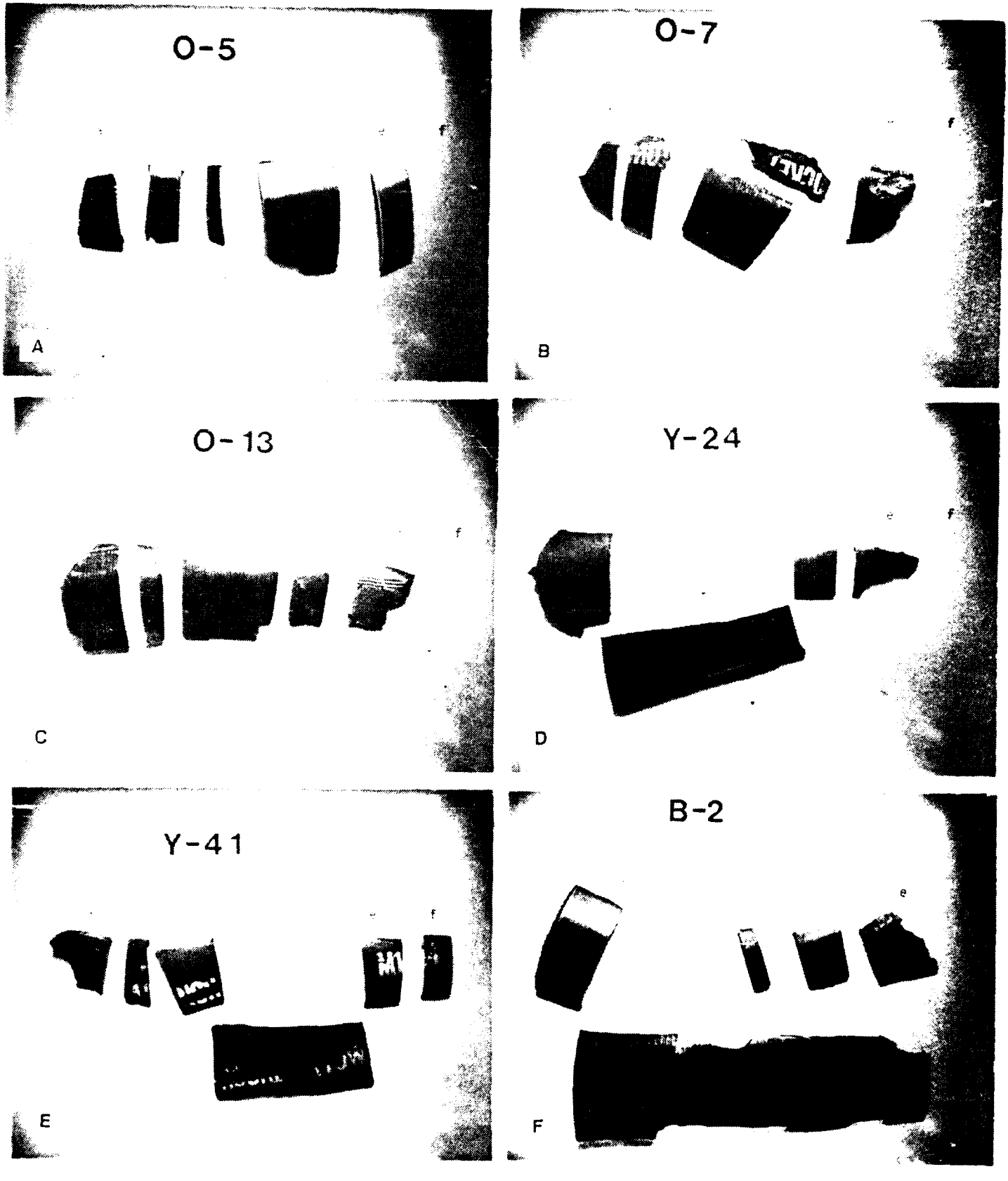

Figure 2. Specimen shapes and sizes after preparation. (a) #O-5 (b) #O-7 (c) #O-13 (d) #Y-24 (e) #Y-41 (f) #B-2.

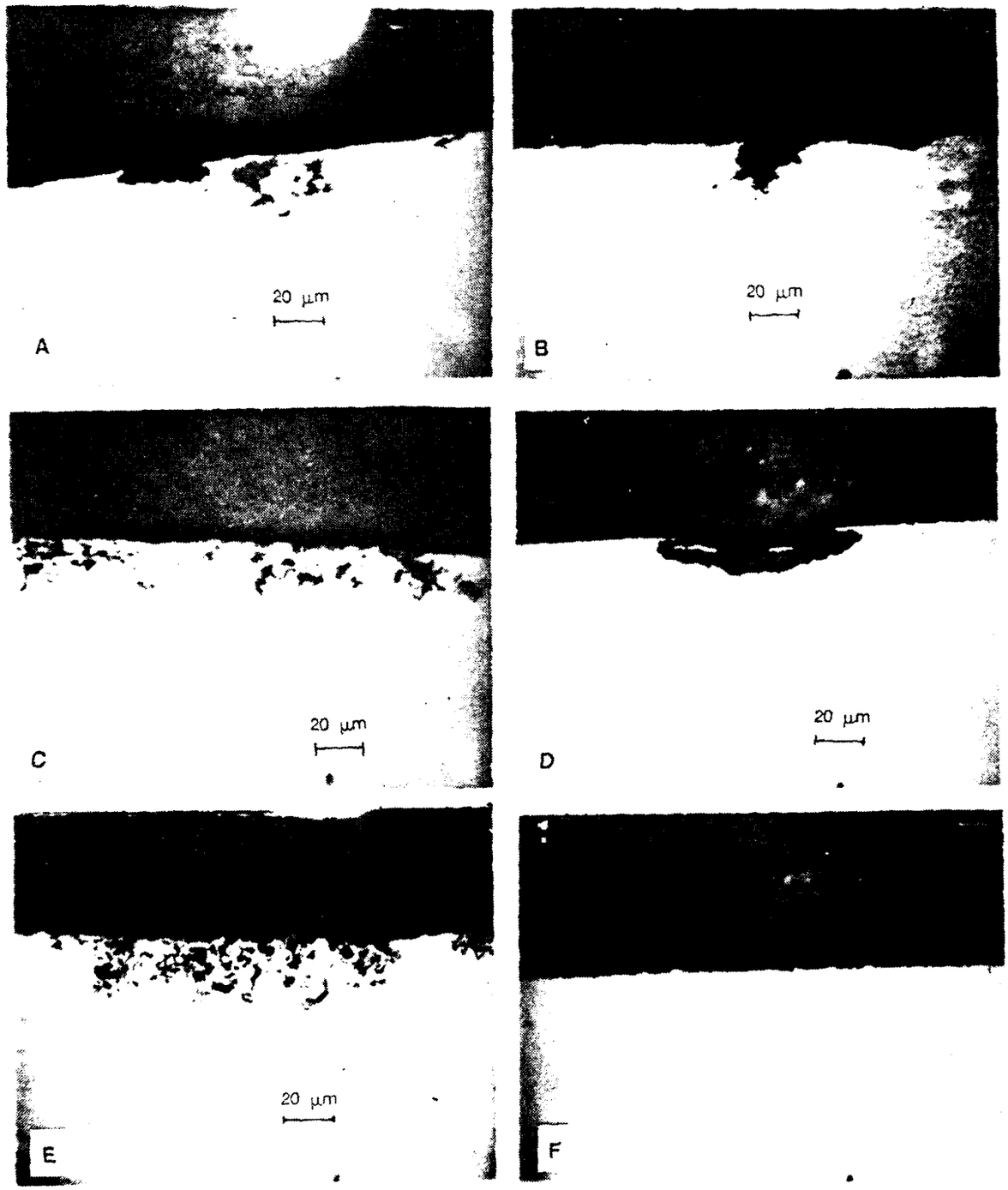

Figure 3. Cross-section micrographs of fracture pieces: (a)#O-5a (b)#O-7e (c)#O-13e (d)#Y-24e (e)#Y-41f (f)#B-2e. Except for (f), many microcracks and fissures are detected. The cracks initiate from corrosion pits or crevices and emanate into 20 micron depth.

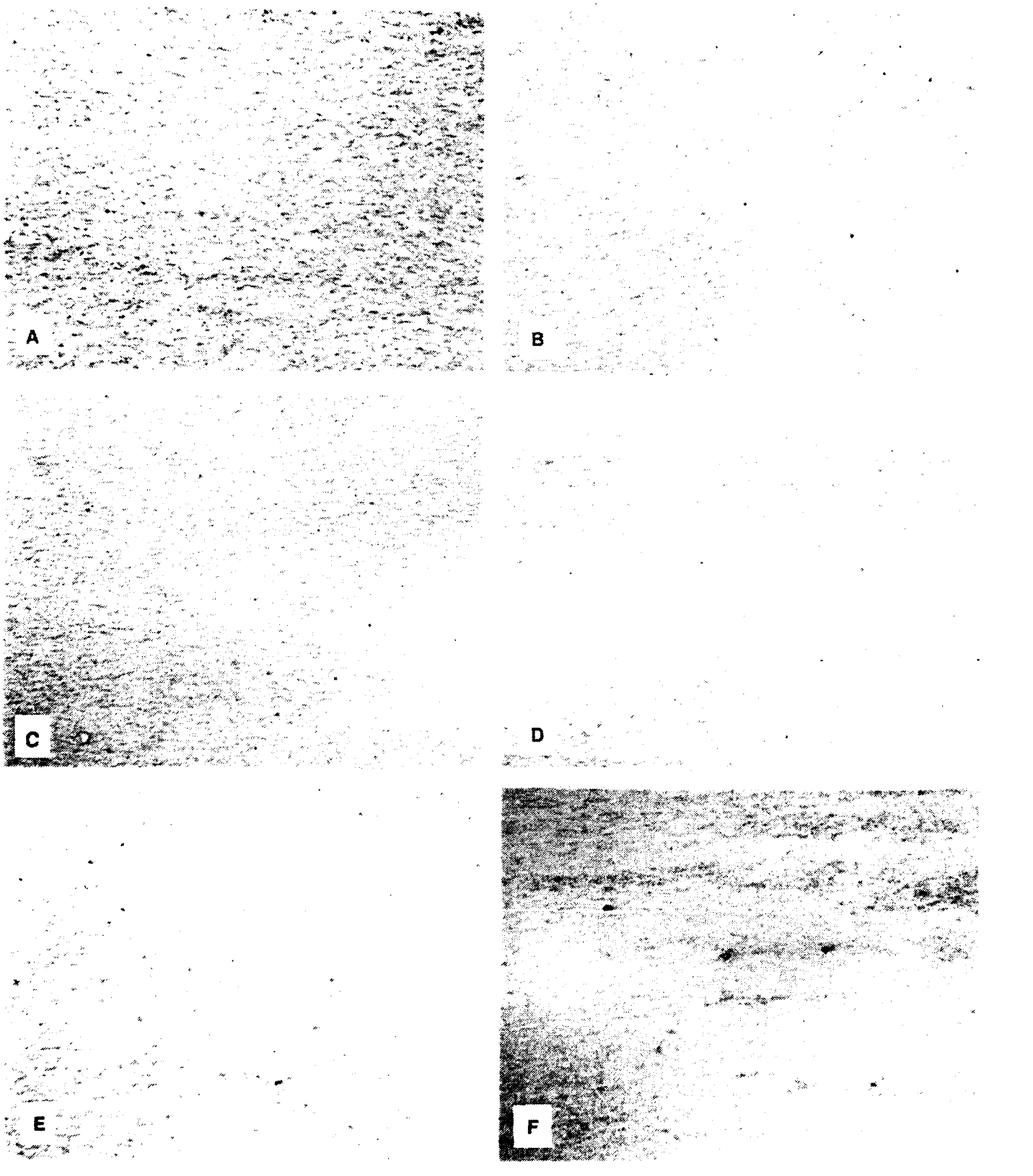

Figure 4. Microstructure of fracture maraging steel samples: (a)#O-5c (b)#O-7b (c)#O-13b (d)#Y-24d (e)#Y-41b (f)#B-2c. Grain structures of #O and #Y samples are similar and that of #B is larger. Grains are elongated on the direction of swaging and rolling. Frame width 150 μm, Mag. 500X.

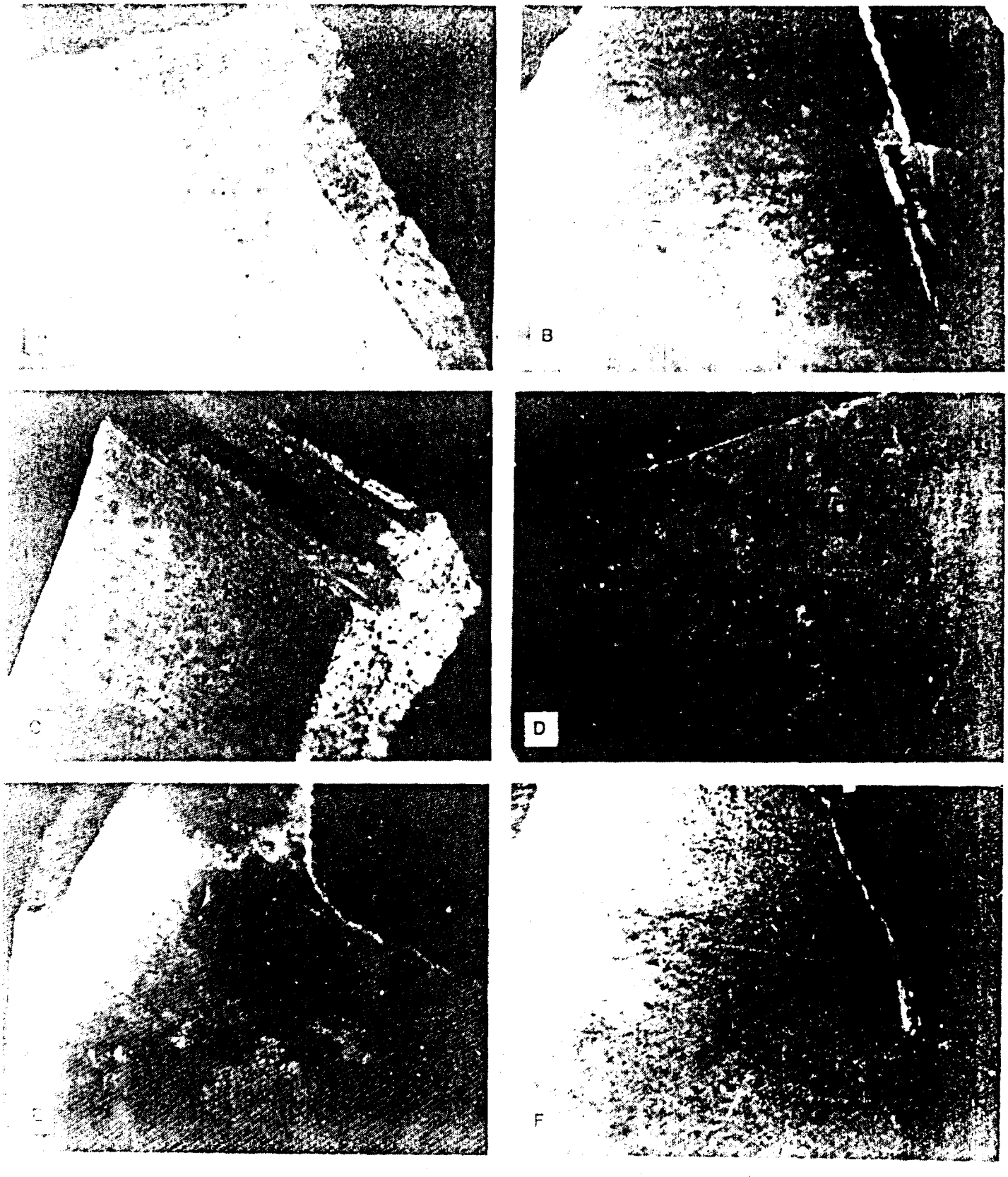
B
C
D
F

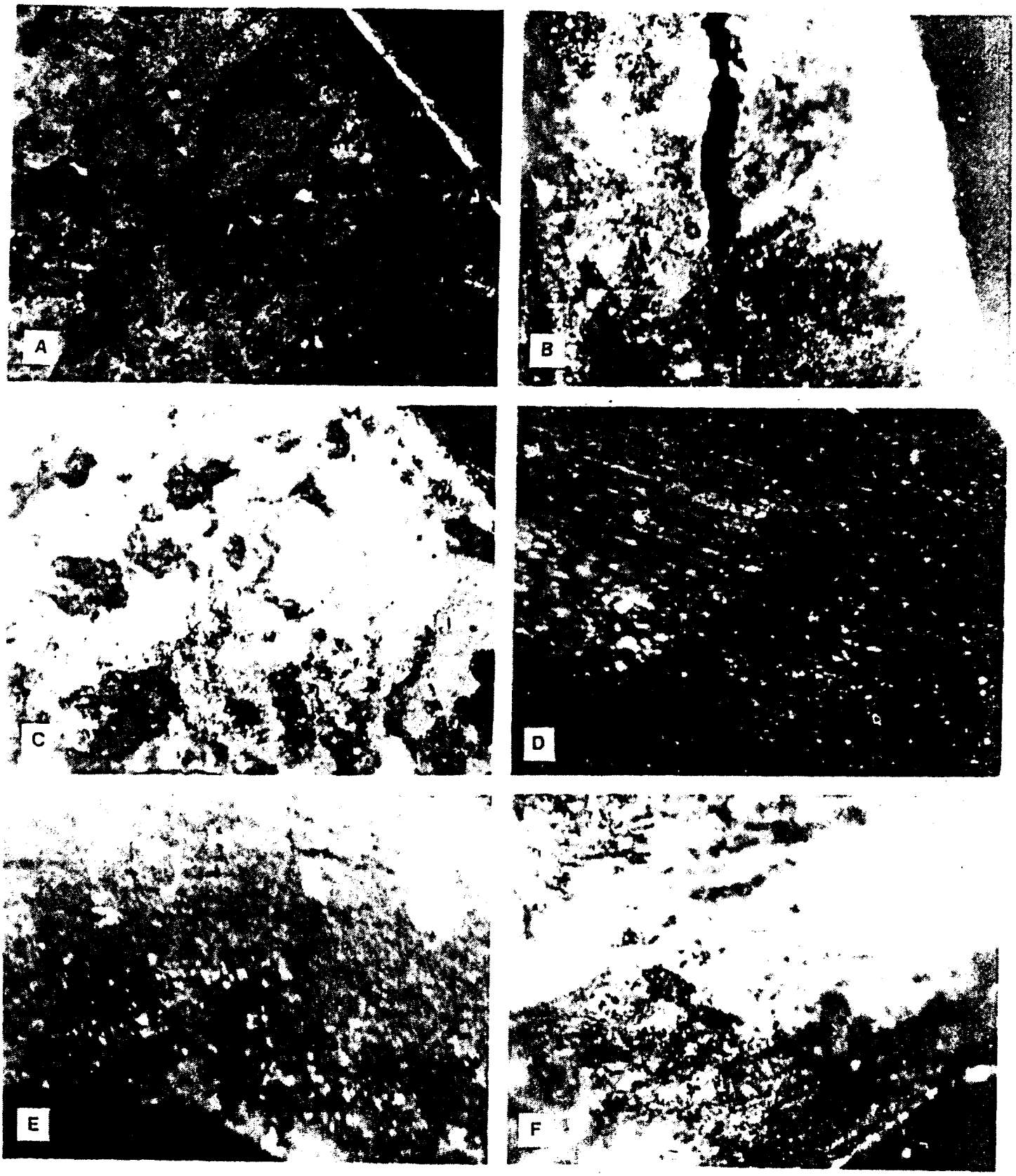

Figure 6 Optical micrographs of fractured surfaces: (a)#O-5a (b)#O-7e (c)#O-13e (d)#Y-24e (e)#Y-41a (f)#B-2e. Most of the surfaces are heavily oxidized and appeared as rusty scales. Strain cracks are visible in (b). Frame width 1.27 mm. Mag. 70X

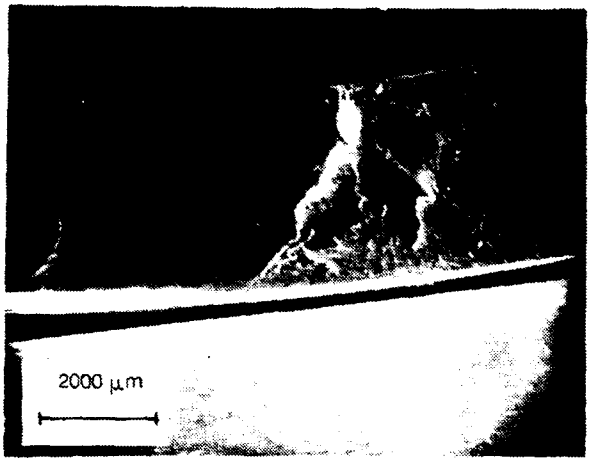

(a) Overview of fracture surface

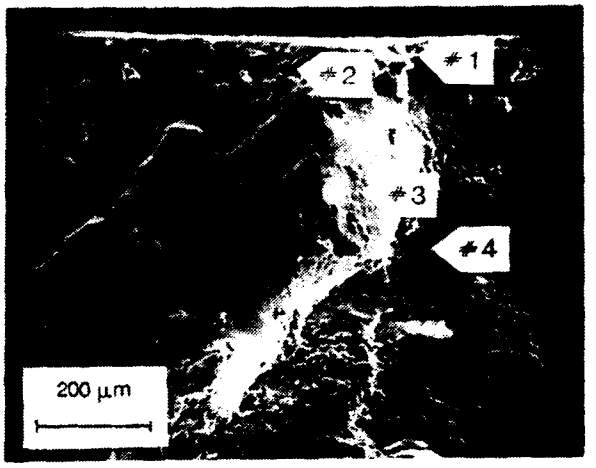

(b) Enlarged fracture surface at a large crack. The spot compositions by EDXA are tabulated in Table 3

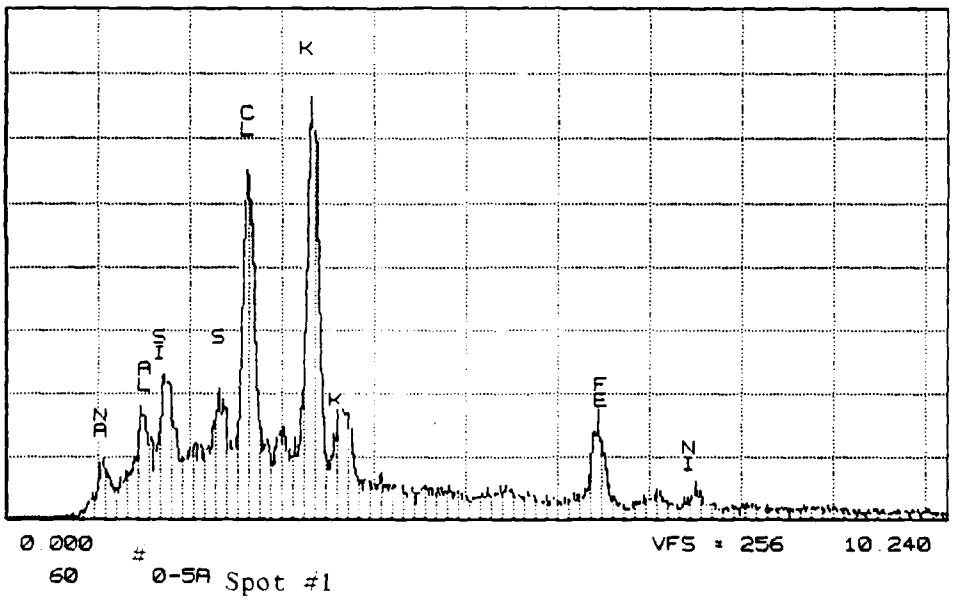

(c) Chemical composition of spot #1 by EDXA near inner wall

Figure 7. SEM of fracture surface #O-5a from Oahu failure.

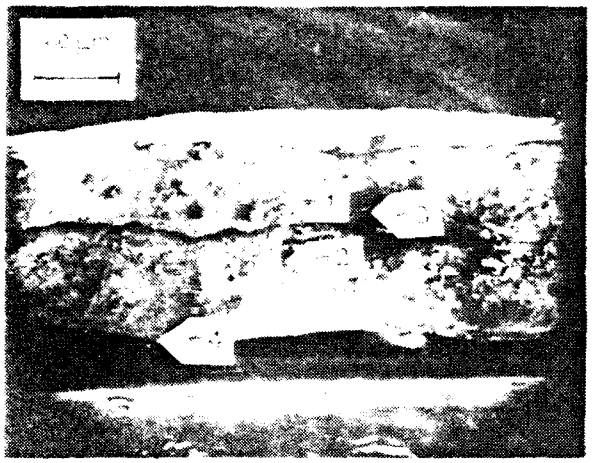

(a) Strain cracks in fracture surface

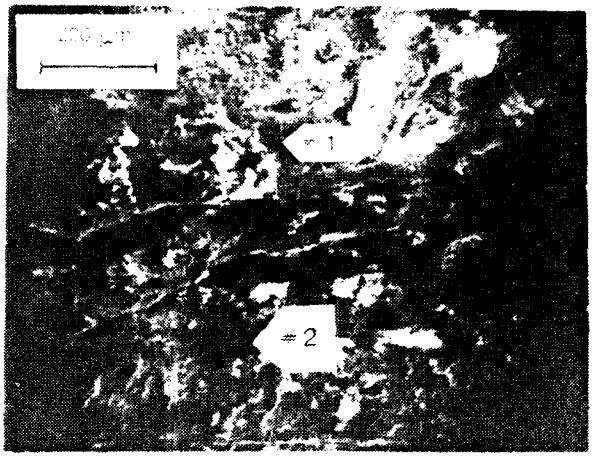

(b) Detailed morphology of strain cracks Spot numbers refer to EDXA chemical constituents

Figure 8. SEM of fracture surface #O-7e from Oahu failure.

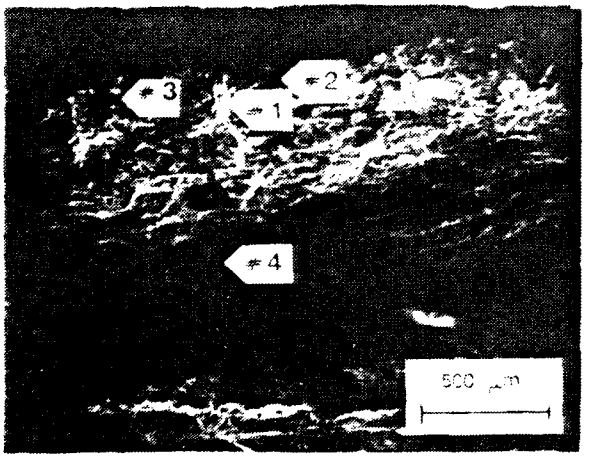

(a) Fracture surface

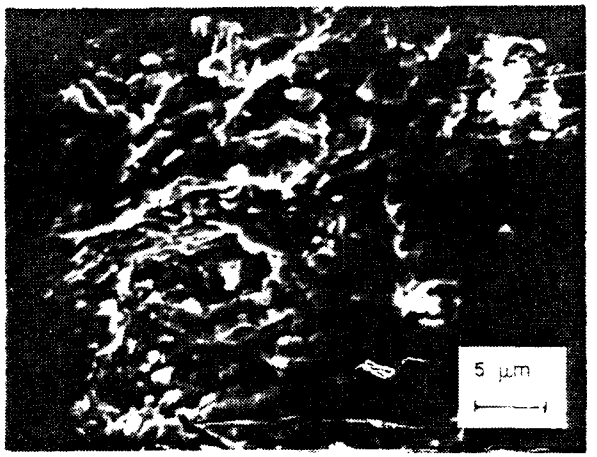

(b) Magnified view of spot #4 on the top of crack edge

Figure 9. SEM of fracture surface #O-13e from Oahu failure.

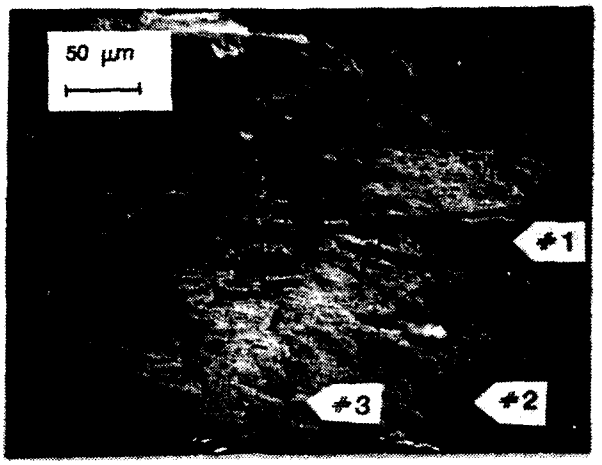

(a) Fracture surface of upper half adjacent to inner wall

(b) Fracture surface of lower half next to outside wall

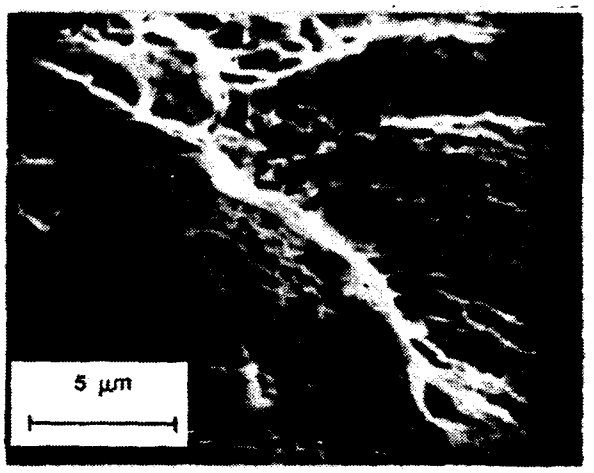

(c) Enlarged area of spot #1 at the rim of a circle crater

Figure 10. SEM of fracture surface #Y-24e from Yakima failure.

(a) Cracked surface at a low glazing angle

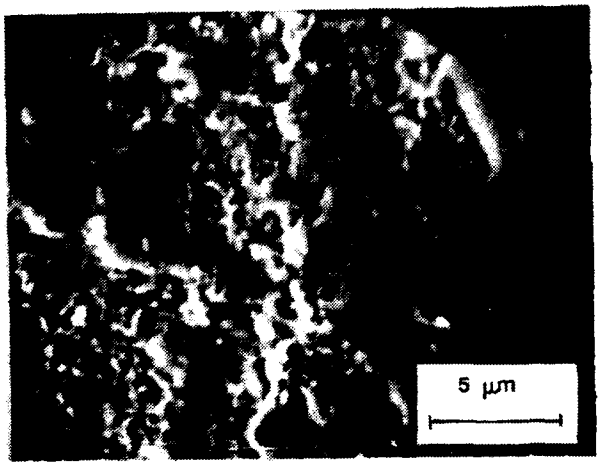

(b) Enlarged view of spot #1 on the tip of crack

Figure 11. SEM of fracture surface #Y-41a from Yakima failure.

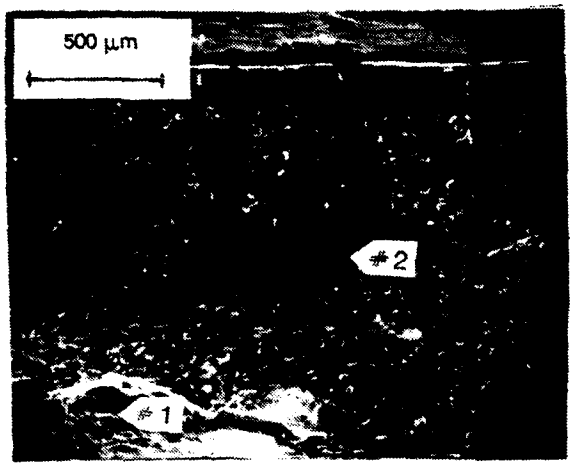

(a) Fracture surface with numerous precipitates

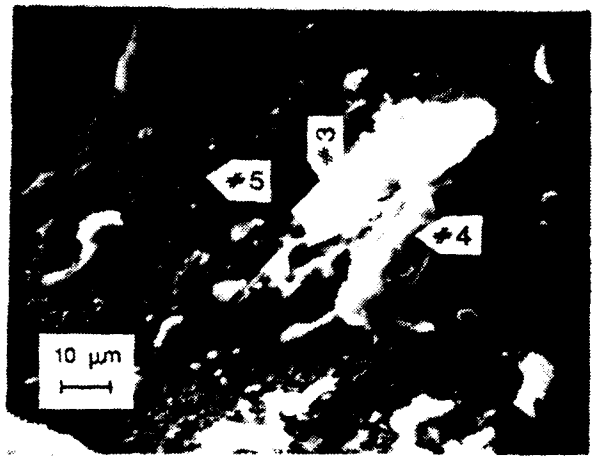

(b) Magnified morphology of spot #2 containing imbedded foreign particles

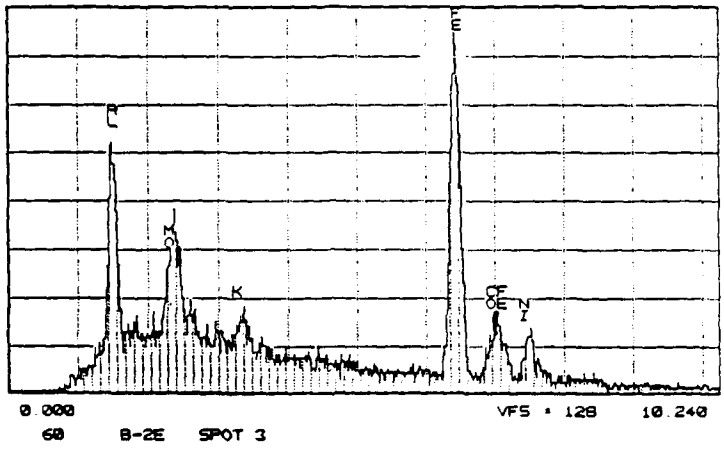

(c) EDXA analysis of spot #3, square particle

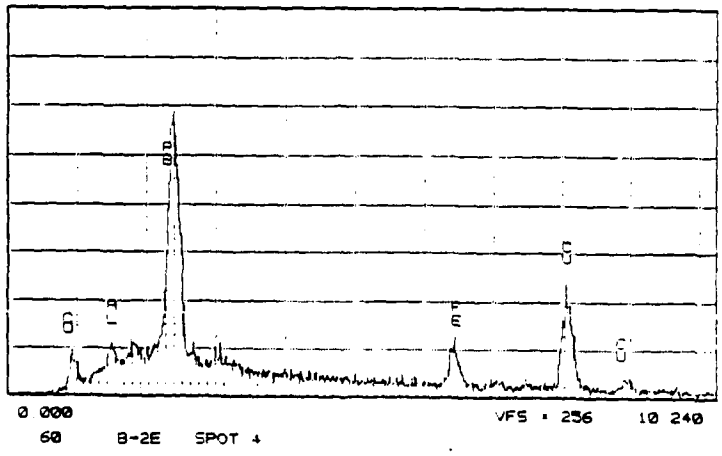

(d) EDXA analysis of spot #4, round particle

Figure 12. SEM of fracture surface #B-2e from blanket test (reference).

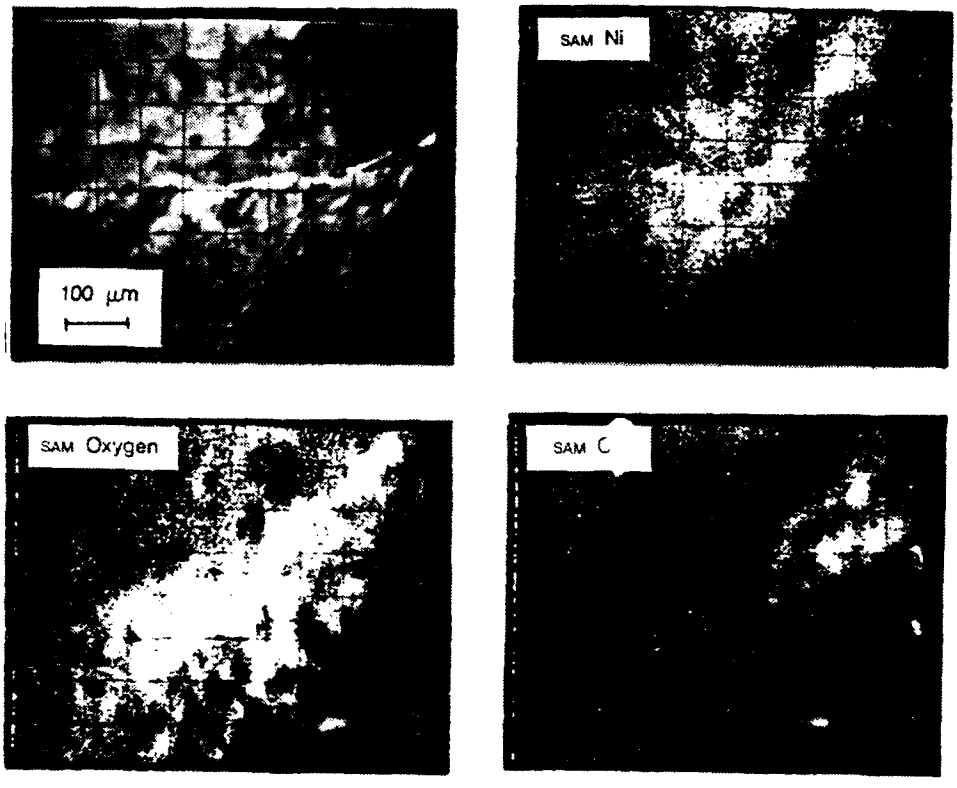

(a) SAM images: reference, nickel, oxygen and chlorine (Cl).
The Cl image is concentrated near the inner wall

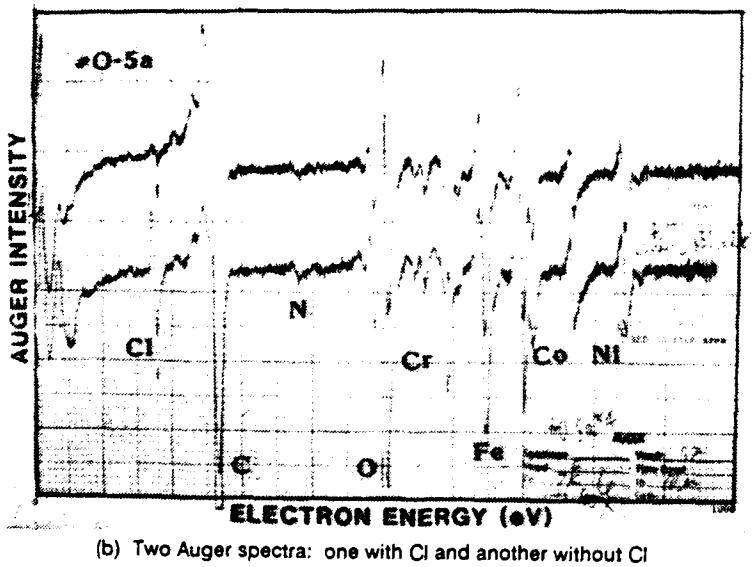

(b) Two Auger spectra: one with Cl and another without Cl

Figure 13. SAM images and AES spectra of fracture surface #O-5a.

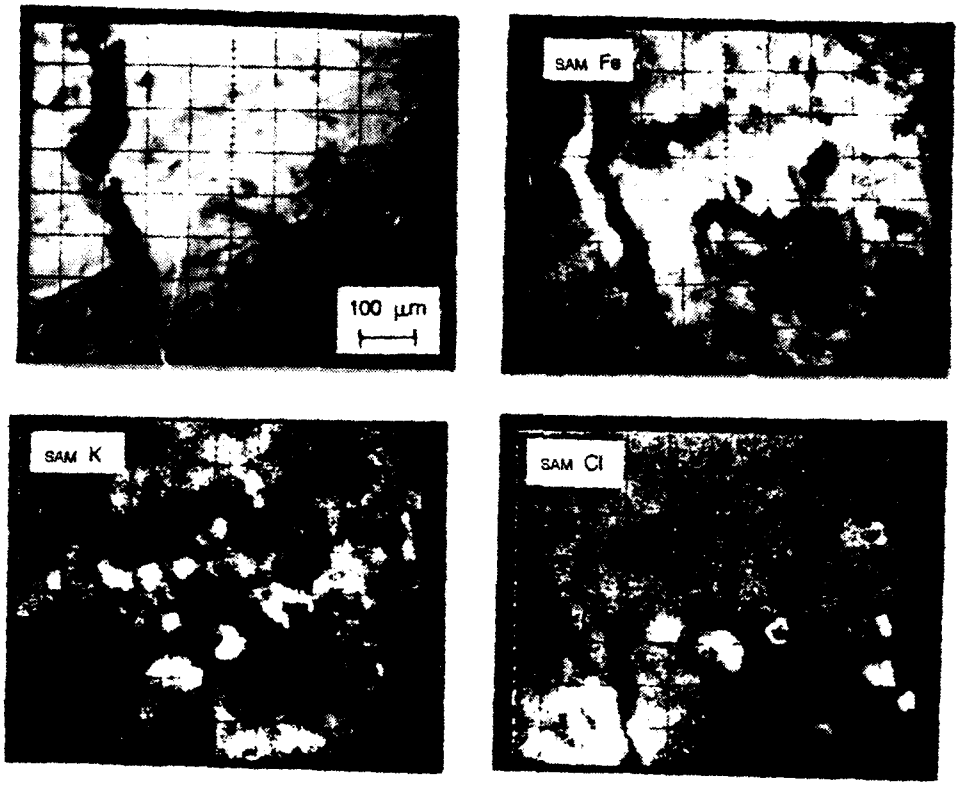

(a) SAM images: reference, iron, potassium (K) and chlorine. The K and Cl are widely scattered

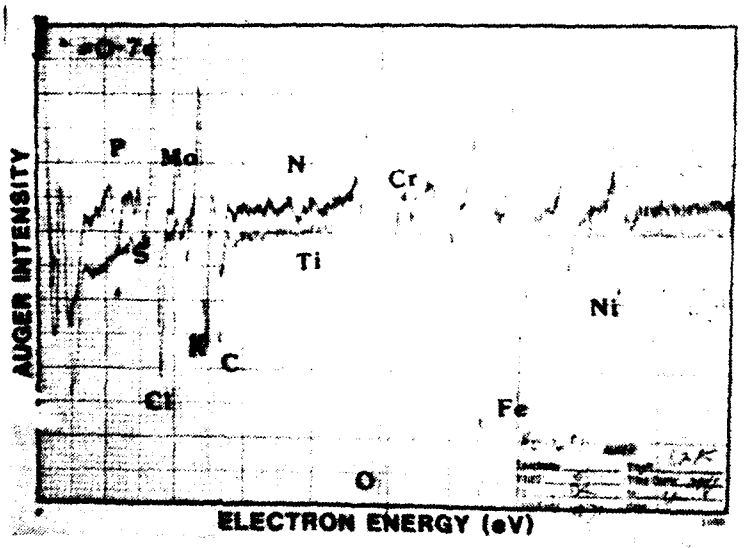

(b) Auger spectra with/without chemical element Cl. The X and Y locations of analyses are indicated

Figure 14. SAM images and AES spectra of fracture surface #O-7c.

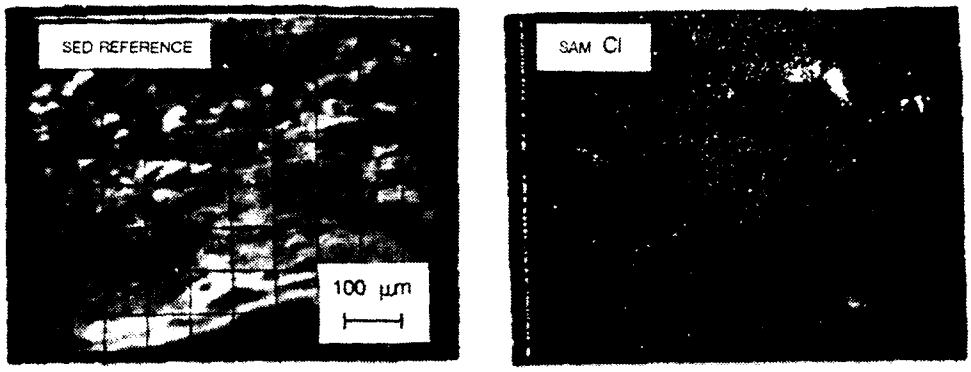

Figure 15. SAM images of fracture surface #O-13e reference and chlorine images. The Cl rich area is not near the inner wall, but is situated at a half wall thickness.

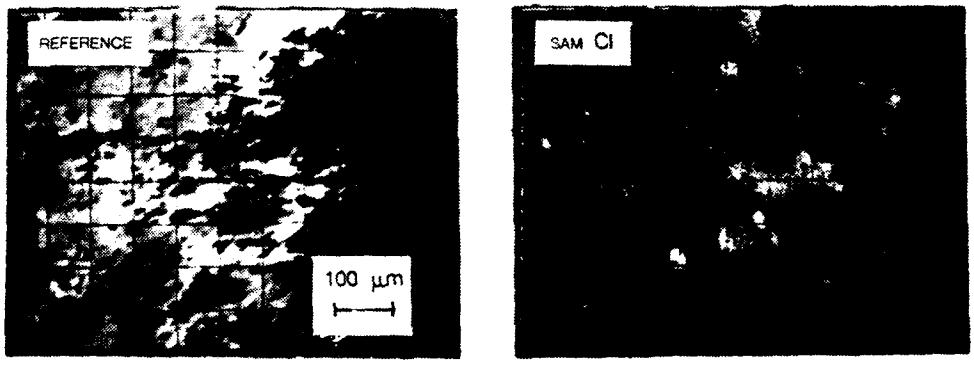

(a) Reference image and SAM chlorine near inner wall

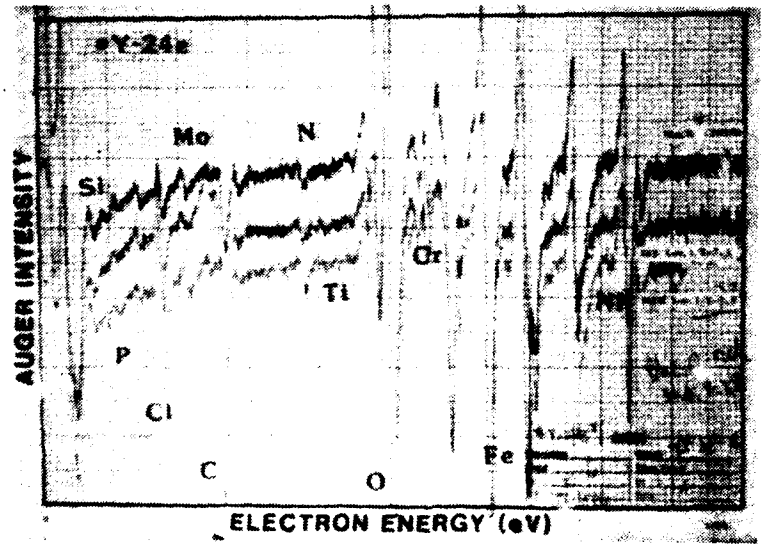

(b) Auger spectra taken at three locations; center, two Cl rich spots

Figure 16. SAM images and AES spectra of fracture surface #Y-24e.

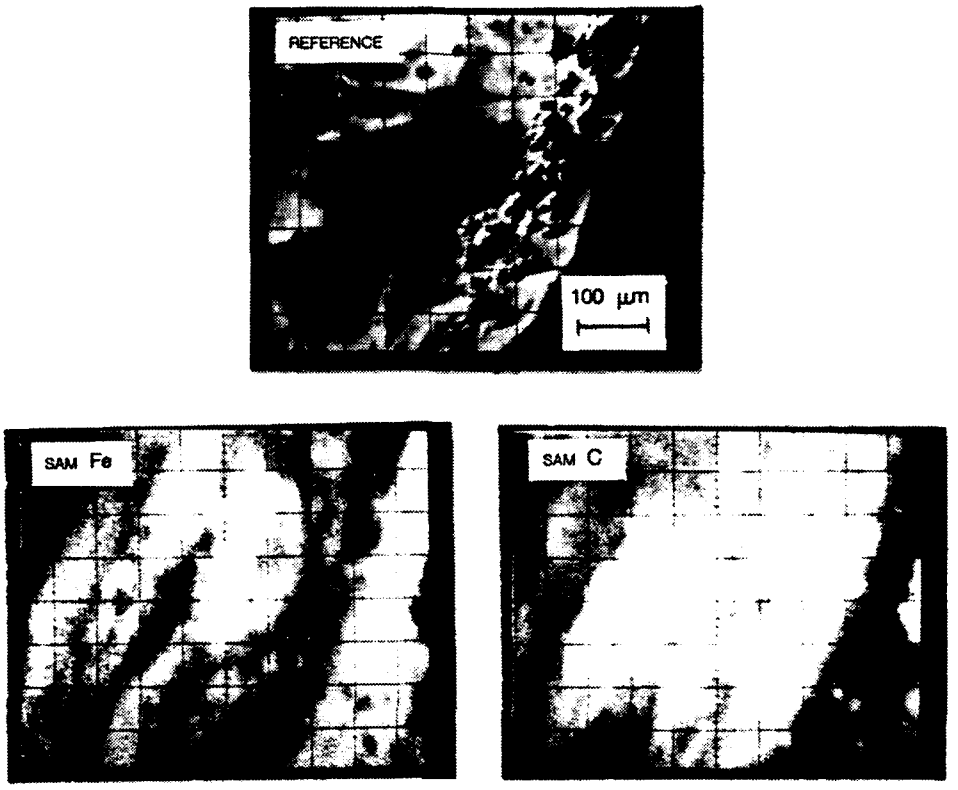

Figure 17. SAM images of fracture surface #Y-41a: reference, iron, and carbon.

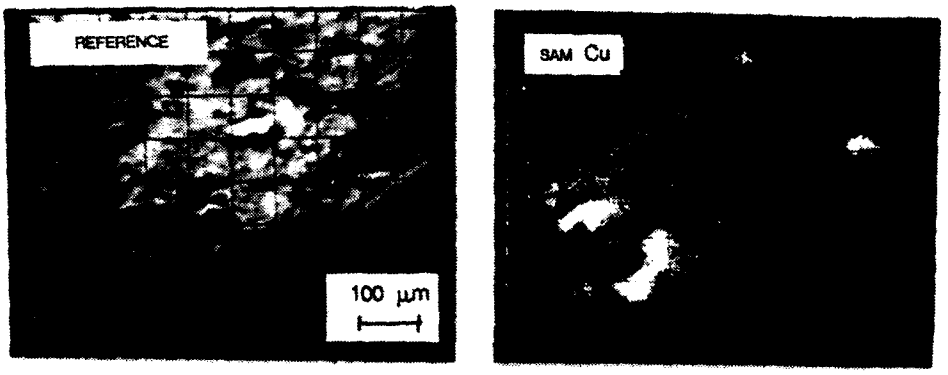

(a) Reference and copper SAM images

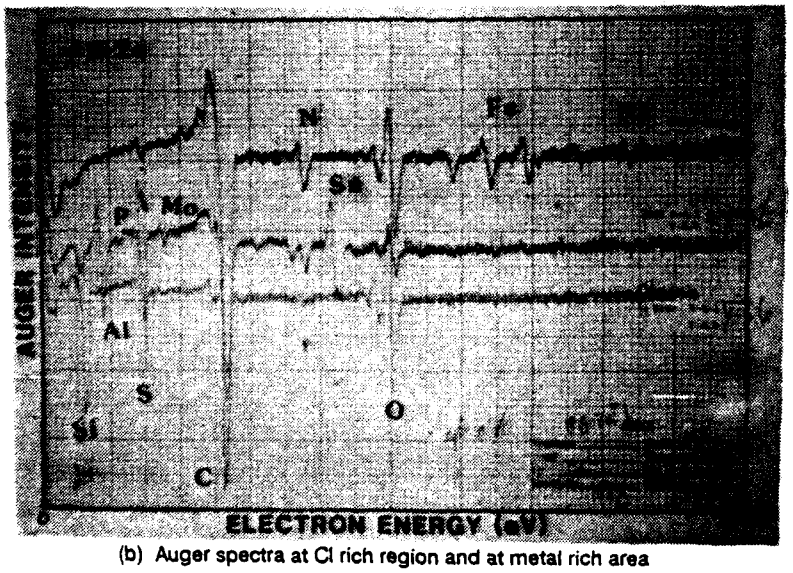

(b) Auger spectra at Cl rich region and at metal rich area

Figure 18. SAM images and AES spectra of fracture surface #B-2a.

DISTRIBUTION LIST

No. of Copies	To
1	Office of the Under Secretary of Defense for Research and Engineering, The Pentagon, Washington, DC 20301
	Commander, U.S. Army Laboratory Command, 2800 Powder Mill Road, Adelphi, MD 20783-1145
1	ATTN: AMSLC-IM-TL
	Commander, Defense Technical Information Center, Cameron Station, Building 5, 5010 Duke Street, Alexandria, VA 22304-6145
2	ATTN: DTIC-FDAC
1	Metals and Ceramics Information Center, Battelle Columbus Laboratories, 505 King Avenue, Columbus, OH 43201
	Commander, Army Research Office, P.O. Box 12211, Research Triangle Park, NC 27709-2211
1	ATTN: Information Processing Office
	Commander, U.S. Army Materiel Command, 5001 Eisenhower Avenue, Alexandria, VA 22333
1	ATTN: AMCLD
	Commander, U.S. Army Materiel Systems Analysis Activity, Aberdeen Proving Ground, MD 21005
1	ATTN: AMXSY-MP, H. Cohen
	Commander, U.S. Army Electronics Research and Development Command, Fort Monmouth, NJ 07703
1	ATTN: AMDSD-L
1	AMDSD-E
	Commander, U.S. Army Missile Command, Redstone Scientific Information Center, Redstone Arsenal, AL 35898-5241
1	ATTN: AMSMI-RKP, J. Wright, Bldg. 7574
1	AMSMI-RD-CS-R/ILL Open Lit
1	AMSMI-RLM
	Commander, U.S. Army Armament, Munitions and Chemical Command, Dover, NJ 07801
2	ATTN: Technical Library
1	AMDAR-LCA, Mr. Harry E. Pebly, Jr., PLASTEC, Director
	Commander, U.S. Army Natick Research, Development, and Engineering Center, Natick, MA 01760
1	ATTN: Technical Library
	Commander, U.S. Army Satellite Communications Agency, Fort Monmouth, NJ 07703
1	ATTN: Technical Document Center
	Commander, U.S. Army Tank-Automotive Command, Warren, MI 4397-5000
1	ATTN: AMSTA-ZSK
2	AMSTA-TSL, Technical Library
	Commander, White Sands Missile Range, NM 88002
1	ATTN: STEWS-WS-VT
	President, Airborne, Electronics and Special Warfare Board, Fort Bragg, NC 28307
1	ATTN: Library
	Director, U.S. Army Ballistic Research Laboratory, Aberdeen Proving Ground, MD 21005
1	ATTN: SLCBR-TSB-S (STINFO)
	Commander, Dugway Proving Ground, Dugway, UT 84022
1	ATTN: Technical Library, Technical Information Division
	Commander, Harry Diamond Laboratories, 2800 Powder Mill Road, Adelphi, MD 20783
1	ATTN: Technical Information Office
	Director, Benet Weapons Laboratory, LCWSL, USA AMCCOM, Watervliet, NY 12189
1	ATTN: AMSMC-LCB-TL
1	AMSMC-LCB-R
1	AMSMC-LCB-RM
1	AMSMC-LCB-RP
	Commander, U.S. Army Foreign Science and Technology Center, 220 7th Street, N.E., Charlottesville, VA 22901
1	ATTN: Military Tech

No. of Copies	To
	Commander, U.S. Army Aeromedical Research Unit, P.O. Box 577, Fort Rucker, AL 36360
1	ATTN: Technical Library
	Director, Eustis Directorate, U.S. Army Air Mobility Research and Development Laboratory, Fort Eustis, VA 23604-5577
1	ATTN: SAVDL-E-MOS (AVSCOM)
	U.S. Army Aviation Training Library, Fort Rucker, AL 36360
1	ATTN: Building 5906-5907
	Commander, U.S. Army Agency for Aviation Safety, Fort Rucker, AL 36362
1	ATTN: Technical Library
	Commander, USACDC Air Defense Agency, Fort Bliss, TX 79916
1	ATTN: Technical Library
	Commander, U.S. Army Engineer School, Fort Belvoir, VA 22060
1	ATTN: Library
	Commander, U.S. Army Engineer Waterways Experiment Station, P. O. Box 631, Vicksburg, MS 39180
1	ATTN: Research Center Library
	Commandant, U.S. Army Quartermaster School, Fort Lee, VA 23801
1	ATTN: Quartermaster School Library
	Naval Research Laboratory, Washington, DC 20375
1	ATTN: Code 5830
2	Dr. G. R. Yoder - Code 6384
	Chief of Naval Research, Arlington, VA 22217
1	ATTN: Code 471
1	Edward J. Morrissey, AFWAL/MLTE, Wright-Patterson Air Force, Base, OH 45433
	Commander, U.S. Air Force Wright Aeronautical Laboratories, Wright-Patterson Air Force Base, OH 45433
1	ATTN: AFWAL/MLC
1	AFWAL/MLLP, M. Forney, Jr.
1	AFWAL/MLBC, Mr. Stanley Schulman
	National Aeronautics and Space Administration, Marshall Space Flight Center, Huntsville, AL 35812
1	ATTN: R. J. Schwinghammer, EH01, Dir, M&P Lab
1	Mr. W. A. Wilson, EH41, Bldg. 4612
	Director, U.S. Army Materials Technology Laboratory, Watertown, MA 02172-0001
2	ATTN: SLCMT-TML
2	Authors

U.S. Army Materials Technology Laboratory
Watertown, Massachusetts 02172-0001
CHEMICAL AND SURFACE CHARACTERIZATION OF TOW MISSILE CASES - Sin-Shong Lin and Wai K. Chin

AD______________
UNCLASSIFIED
UNLIMITED DISTRIBUTION

Technical Report MTL TR 88-48, December 1988, 26 pp-illus-tables

Key Words
Failure analysis
Surface analysis
Missile casing

Six fragments from TOW missile motor case failures were examined by optical microscopy, scanning electron microscopy, scanning Auger microprobe, and bulk chemical composition analyses. The investigation has identified some positive evidence of corrosion cracking. The inner wall surfaces of the motor casings were corroded and many micro cracks emanating from corrosion pits and oxidized scales were observed. Chlorine was found to be a major element existing in the cracks. Aside from the mechanical strength of the steel, the failure of the motor casings might be attributed to stress corrosion cracking.

U.S. Army Materials Technology Laboratory
Watertown, Massachusetts 02172-0001
CHEMICAL AND SURFACE CHARACTERIZATION OF TOW MISSILE CASES - Sin-Shong Lin and Wai K. Chin

AD______________
UNCLASSIFIED
UNLIMITED DISTRIBUTION

Technical Report MTL TR 88-48, December 1988, 26 pp-illus-tables

Key Words
Failure analysis
Surface analysis
Missile casing

Six fragments from TOW missile motor case failures were examined by optical microscopy, scanning electron microscopy, scanning Auger microprobe, and bulk chemical composition analyses. The investigation has identified some positive evidence of corrosion cracking. The inner wall surfaces of the motor casings were corroded and many micro cracks emanating from corrosion pits and oxidized scales were observed. Chlorine was found to be a major element existing in the cracks. Aside from the mechanical strength of the steel, the failure of the motor casings might be attributed to stress corrosion cracking.

U.S. Army Materials Technology Laboratory
Watertown, Massachusetts 02172-0001
CHEMICAL AND SURFACE CHARACTERIZATION OF TOW MISSILE CASES - Sin-Shong Lin and Wai K. Chin

AD______________
UNCLASSIFIED
UNLIMITED DISTRIBUTION

Technical Report MTL TR 88-48, December 1988, 26 pp-illus-tables

Key Words
Failure analysis
Surface analysis
Missile casing

Six fragments from TOW missile motor case failures were examined by optical microscopy, scanning electron microscopy, scanning Auger microprobe, and bulk chemical composition analyses. The investigation has identified some positive evidence of corrosion cracking. The inner wall surfaces of the motor casings were corroded and many micro cracks emanating from corrosion pits and oxidized scales were observed. Chlorine was found to be a major element existing in the cracks. Aside from the mechanical strength of the steel, the failure of the motor casings might be attributed to stress corrosion cracking.

U.S. Army Materials Technology Laboratory
Watertown, Massachusetts 02172-0001
CHEMICAL AND SURFACE CHARACTERIZATION OF TOW MISSILE CASES - Sin-Shong Lin and Wai K. Chin

AD______________
UNCLASSIFIED
UNLIMITED DISTRIBUTION

Technical Report MTL TR 88-48, December 1988, 26 pp-illus-tables

Key Words
Failure analysis
Surface analysis
Missile casing

Six fragments from TOW missile motor case failures were examined by optical microscopy, scanning electron microscopy, scanning Auger microprobe, and bulk chemical composition analyses. The investigation has identified some positive evidence of corrosion cracking. The inner wall surfaces of the motor casings were corroded and many micro cracks emanating from corrosion pits and oxidized scales were observed. Chlorine was found to be a major element existing in the cracks. Aside from the mechanical strength of the steel, the failure of the motor casings might be attributed to stress corrosion cracking.